Supplementary Information for:

Nanoscale Optomechanical Actuators for Controlling Mechanotransduction in Living Cells

Zheng Liu[1*], Yang Liu[1*], Yuan Chang[1], Hamid Reza Seyf[2], Asegun Henry[2,3], Alexa L. Mattheyses[4], Kevin Yehl[1], Yun Zhang[1], Zhuangqun Huang[5], Khalid Salaita[1+]

[1]Department of Chemistry, Emory University, Atlanta, GA, USA.
[2]Georgia Institute of Technology, George W. Woodruff School of Mechanical Engineering Atlanta, GA, USA.
[3]Georgia Institute of Technology, School of Materials Science and Engineering, Atlanta, GA, USA.
[4]Department of Cell Biology, Emory University School of Medicine, Atlanta, GA, USA.
[5]Bruker Nano Surfaces Division, Santa Barbara, CA, USA.
[*]These authors contributed equally to this work
[+]Correspondence should be addressed to K.S. (k.salaita@emory.edu

Table of content

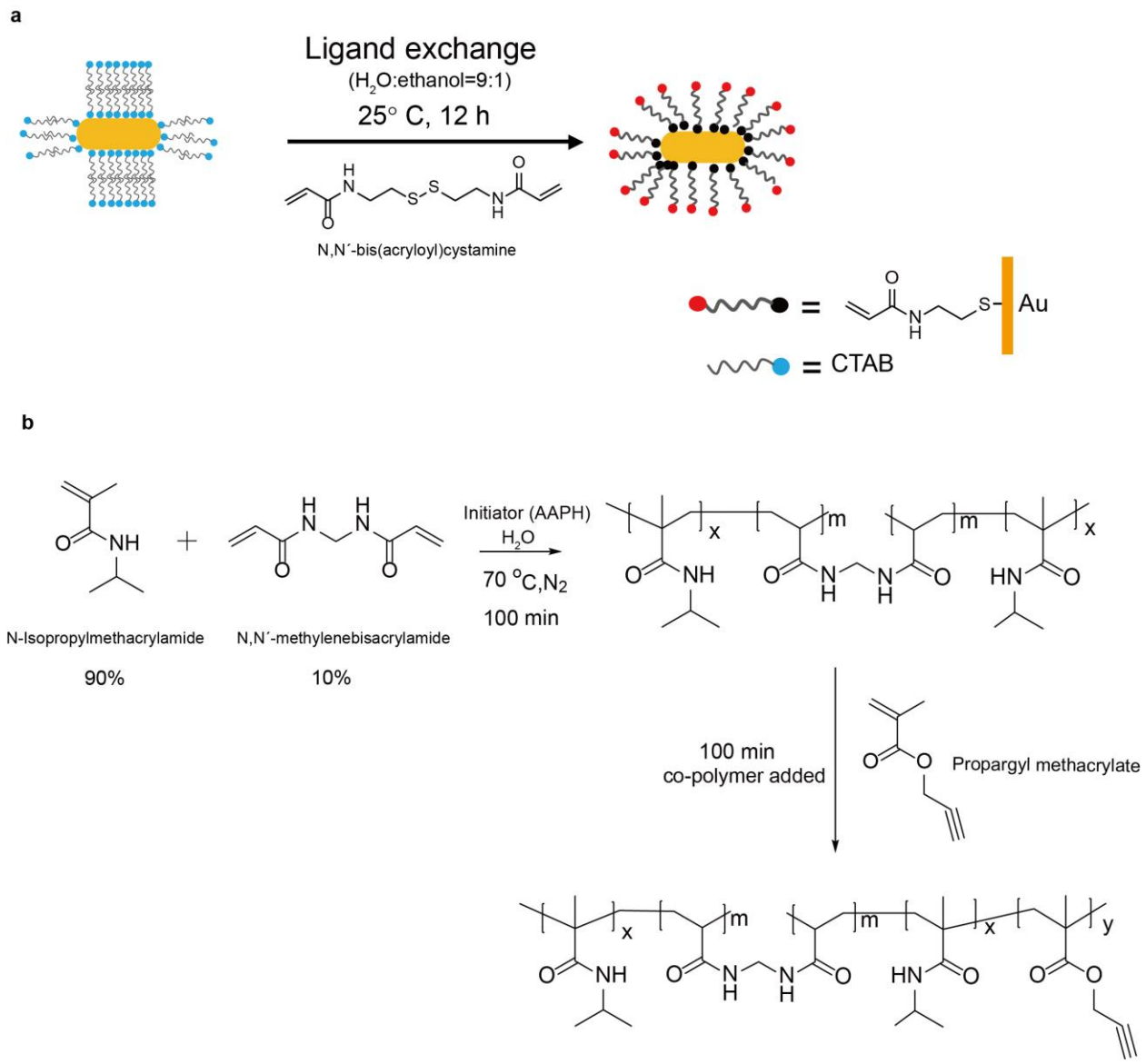

Supplementary Figure 1: Schematic illustration of the preparation of pNIPMAm coated gold nanorods through a two-step procedure

(**a**) Surface functionalization of gold nanorods with alkene functional groups using N,N′-bis(acryloyl)cystamine (BAC). (**b**) Synthetic procedure for polymerization of gold nanorods coated with pNIPMAm polymer. For more details, see Online Methods.

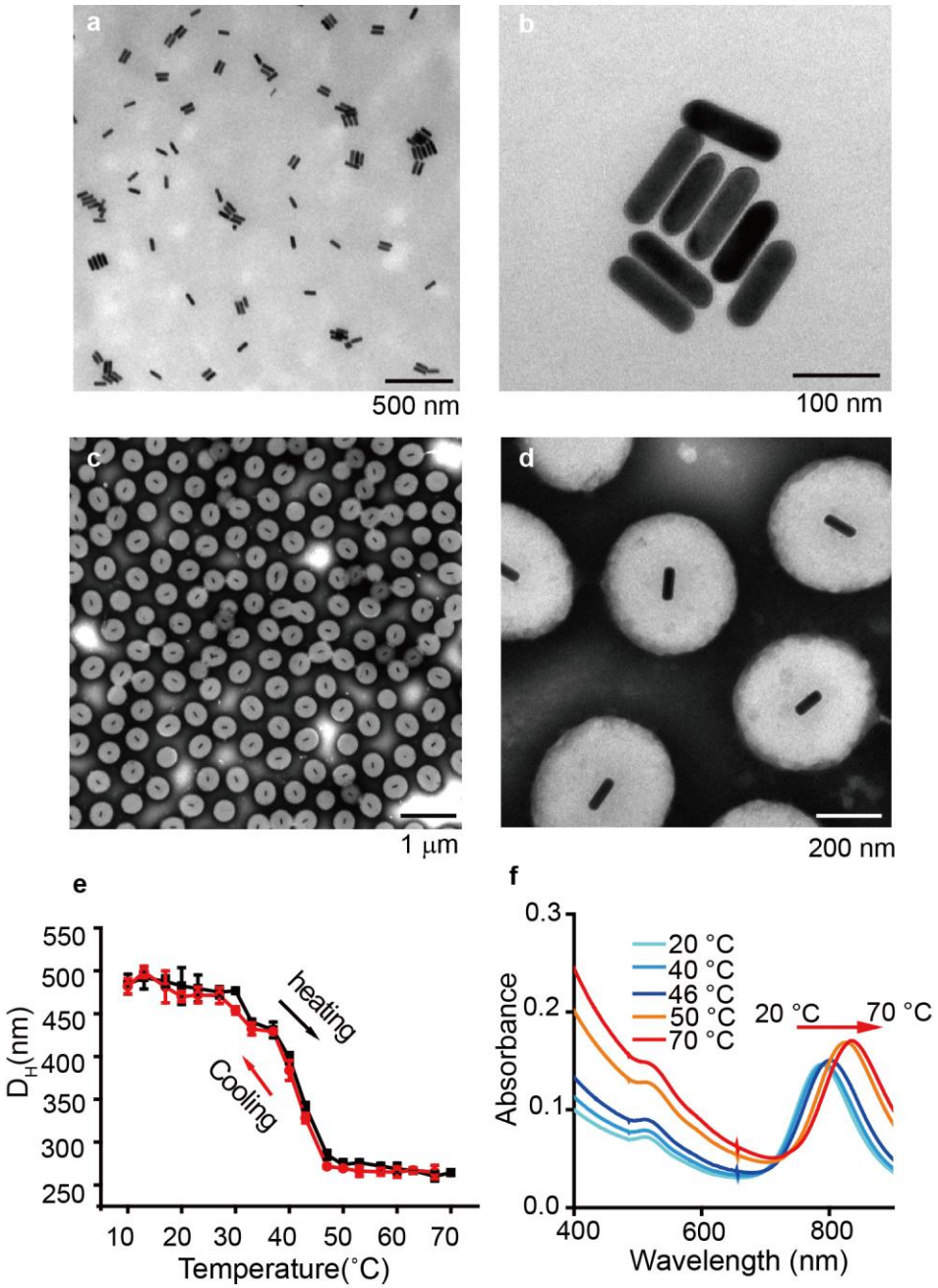

Supplementary Figure 2: Characterization of OMA particles

(**a, b**) Representative TEM images of the gold nanorods (~25 nm × 100 nm) with a LSPR maxima at 785 nm. (**c, d**) Representative TEM images of OMA nanoparticles. Please note that because TEM is conducted under vacuum, TEM images may underestimate the size of the hydrated polymer shell. (**e**) Temperature-controlled DLS measurements reporting the hydrodynamic diameter of OMA nanoparticles as a function of temperature. (**f**) Temperature-dependent vis-NIR absorption spectra of OMA nanoparticles (from 20 to 70°C). At T>42 °C, the Vis-NIR spectra showed an increase in extinction for λ<650 nm, accompanied by a red shift and enhancement in the NIR λ_{max}. The shift in the NIR peak is driven by an increase in the refractive index of the polymer shell following particle collapse, while the increase in extinction at λ<650 nm is likely due to additional scattering above the phase-transition temperature.

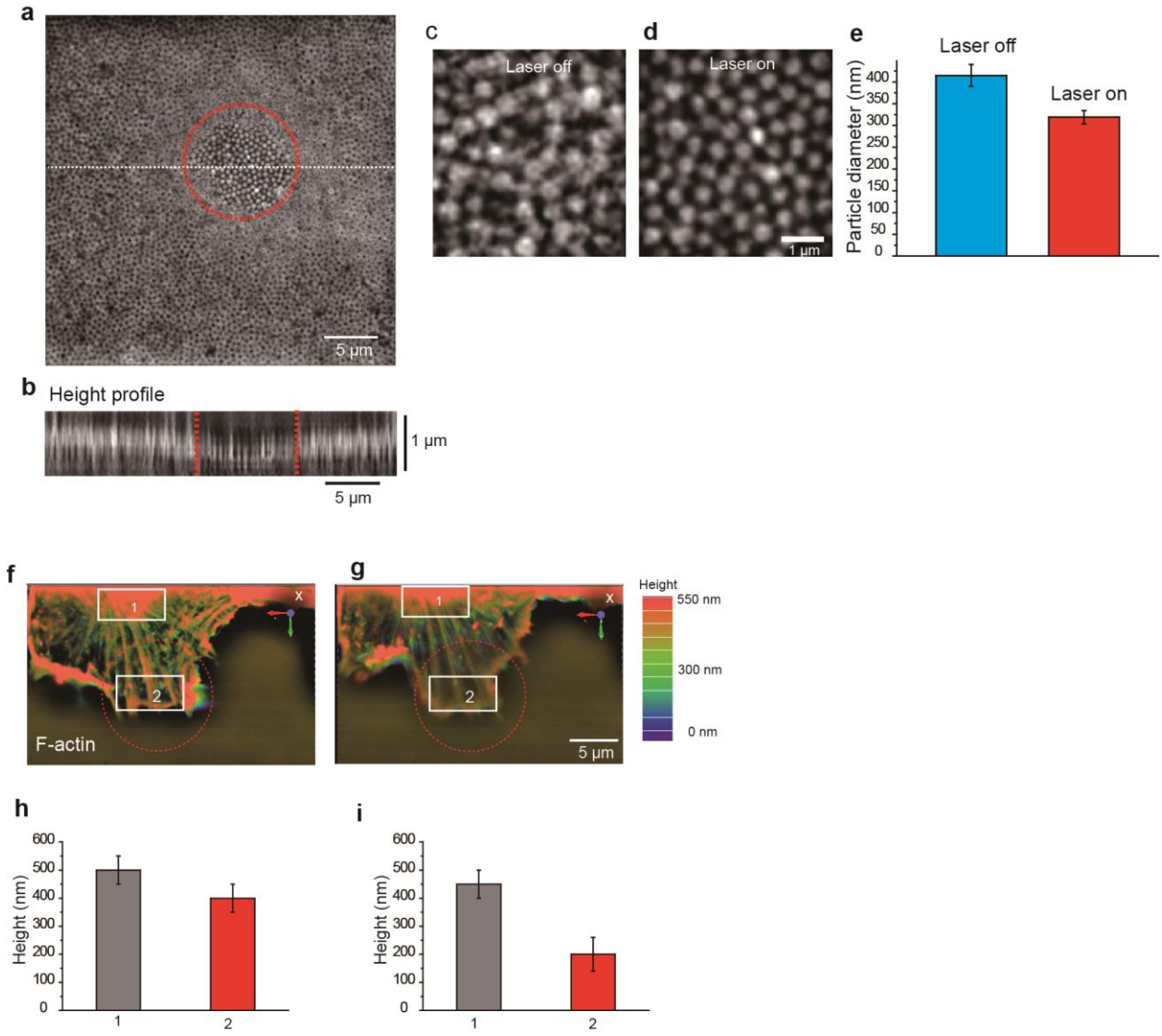

Supplementary Figure 3: 3D-SIM of OMA particles and the F-actin network upon NIR illumination

(a) Representative 3D-SIM image of OMA nanoparticles labeled with Alexa 488 and irradiated using a 785 nm NIR laser at 113 µW µm^{-2}. The image is taken from a single z-position where the collapsed particles (within dotted red circle) were optimally focused. Data was collected in DI water at room temperature. The final 3D image was reconstructed from a stack of 27 individual SIM images starting from the coverslip with 50 nm step size (each 2D SIM image was reconstructed from 15 acquisitions). **(b)** Side view of a single *x*-*z* cross-section cut through the white dashed line shown in **a**. (**c**-**d**) Representative zoom-in SIM images of OMA nanoparticles before and after NIR illumination. (**e**) Plot displaying the FWHM of OMA particles (from *n*=10 particles for each group) before and after NIR illumination. (**f**-**g**) 3D SIM images of a live NIH 3T3 cell expressing LifeAct-mCherry before and after OMA actuation (111 µW µm^{-2}, 100% duty cycle). The red dashed circle represents the region of NIR illumination. (**h**-**i**) Plots display the average heights of F-actin network from the denoted regions of interest 1 and 2 indicated by white boxes in **f** and **g**. The error bar for each data point represents the standard deviation of heights measured by line scan analysis from *n*= 5 lines.

Note that there is minimal actin recruitment within the region of illumination (red dashed circle) in **g.** This is because the 3D-SIM experiments were conducted using steady state illumination (100% duty cycle, 0 Hz). As indicated in the main text and **Supplementary Figure 16 and 17**, cyclic mechanical stimulation is required for actin recruitment and FA growth.

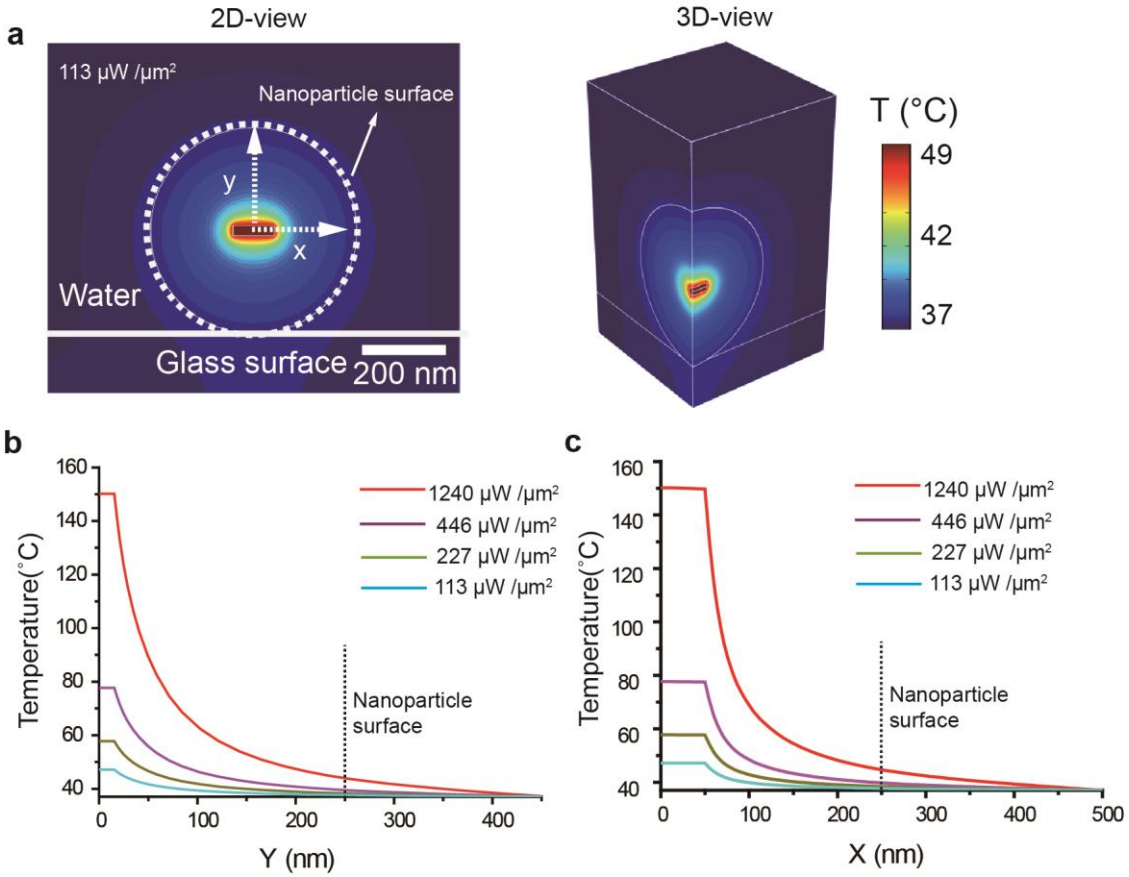

Supplementary Figure 4: 3D-finite element simulation of the heat distribution in a OMA nanoparticle irradiated with 785 nm IR laser beam

(**a**) 3D-finite element simulation of the heat distribution in a OMA nanoparticle irradiated with 785 nm IR laser beam at a power density of 113 μW μm^{-2} in water. (**b, c**) Plots showing cross-sectional temperature profiles along the short (Y) and long (X) axis of a single Au nanorod irradiated with 785 nm IR laser beam for four different power densities (1240, 446, 227,113 μW μm^{-2}).

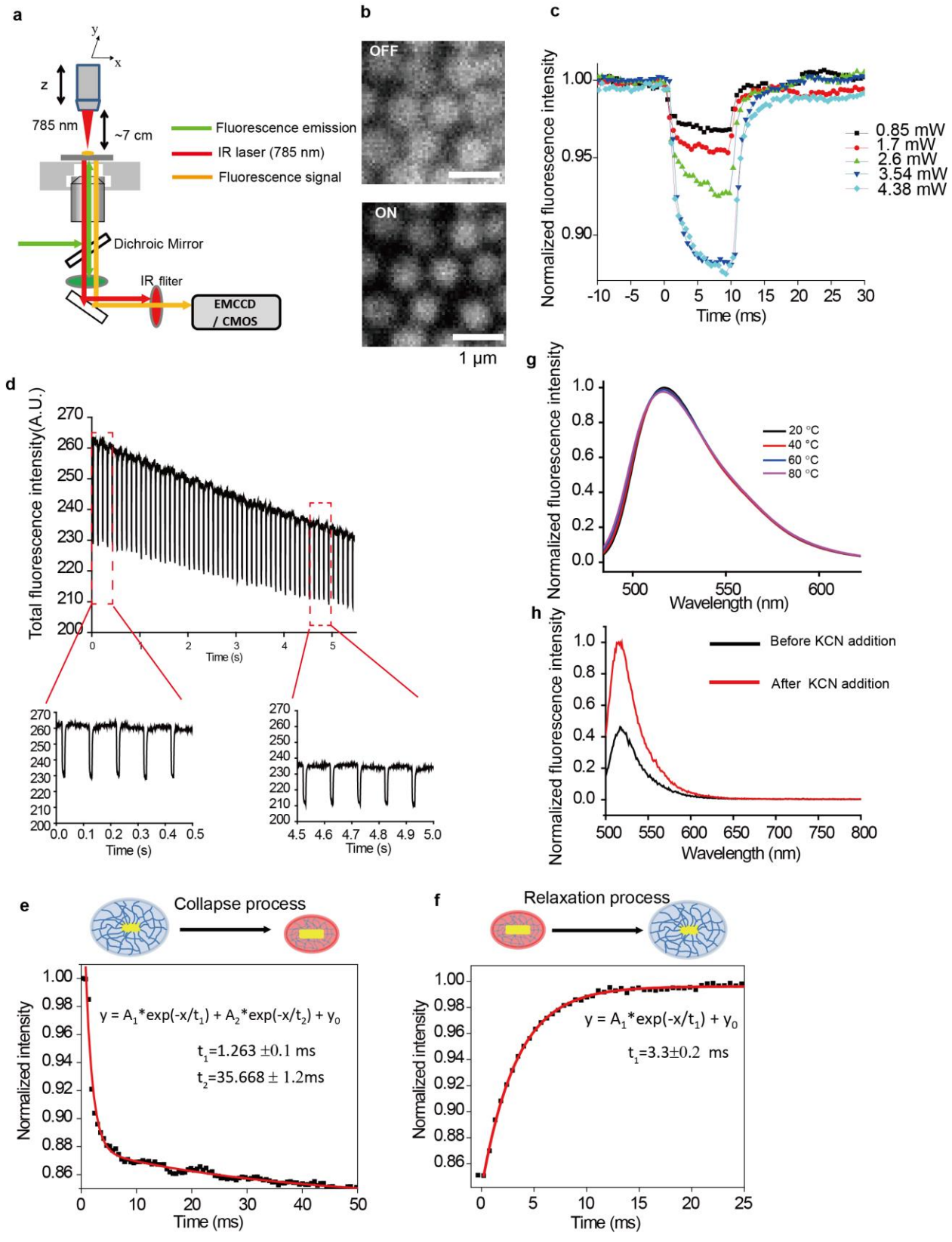

Supplementary Figure 5: Determination of the collapse and relaxation dynamics of OMA nanoparticles

(**a**) Schematic of the experimental setup used for controlling the collapse of OMA nanoparticles. A near-infrared diode laser (Schäfter+Kirchhoff, Hamburg, Germany) was mounted using the standard darkfield condenser accessory provided by Nikon. (**b**) Representative fluorescence images of OMA nanoparticles labeled with Alexa 488 and captured by a sCMOS camera (Zyla 4.2 sCMOS, Andor Technologies Ltd., UK) at 1800 fps while NIR laser was switched between the on and off state. Data was collected in DI water at 37°C. (**c**) Fluorescence versus time plot showing kinetics of OMA particle collapse and subsequent relaxation when the surface was excited at different NIR laser power intensities (10 Hz, 10% duty cycle). (d) A plot showing the total fluorescence intensity of OMA nanoparticles as a function of time while the NIR laser is operating at 10 Hz frequency and 10% duty cycle. OMA particle collapse and subsequent relaxation was highly reversible and could be sustained for at least 10^6 cycles (See online methods). (**e**) A biexponential decay fit of a typical NIR-induced polymer collapse in the time domain of 0–50 ms where the τ_1 and τ_2 were 1.2 and 35 ms, respectively. (**f**) The particle collapse relaxation process can be fit to a single-exponential rise, τ_1 which was 3.3 ms. (**f**) Alexa fluor 488 fluorescence temperature dependence in the range of 20–80 °C in Milli-Q water. The results show that Alexa fluor 488 is a temperature independent dye. (**g**) Normalized fluorescence intensity of OMA nanoparticles labeled with Alexa fluor 488 dye before (black) and after (red) dissolution of the gold nanorods. Taken together, this indicates that the ~15% decrease in fluorescence in **Fig. 1f** and **Supplementary Figure 5c, d, e and f** is primarily due to quenching by the Au nanorod core upon particle collapse.

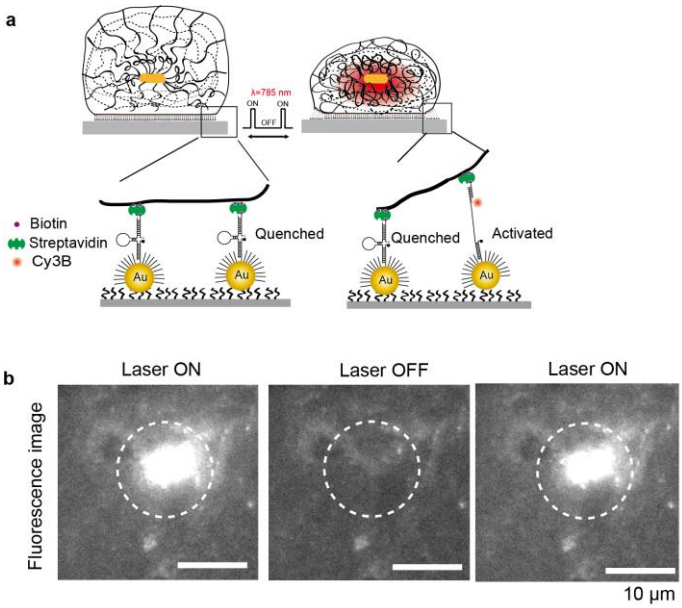

Supplementary Figure 6: Estimation of OMA nanoparticle collapse-driven force using molecular tension sensor

(**a**) Schematic showing the approach used to estimate the force generated by OMA nanoparticle collapse using DNA hairpin based molecular tension sensor. (**b**) Representative fluorescence images of DNA-AuNP tension sensor while NIR laser was switched between the on and off state.

Note that temperature measurements confirm that DNA unfolding was mechanically driven and not thermal (melting temperature of hairpin= 81.3 °C).This suggests that the particle collapse exerts a force per ligand that is greater than 13 pN (force response threshold), but below the ~50 pN force required to shear DNA duplexes.

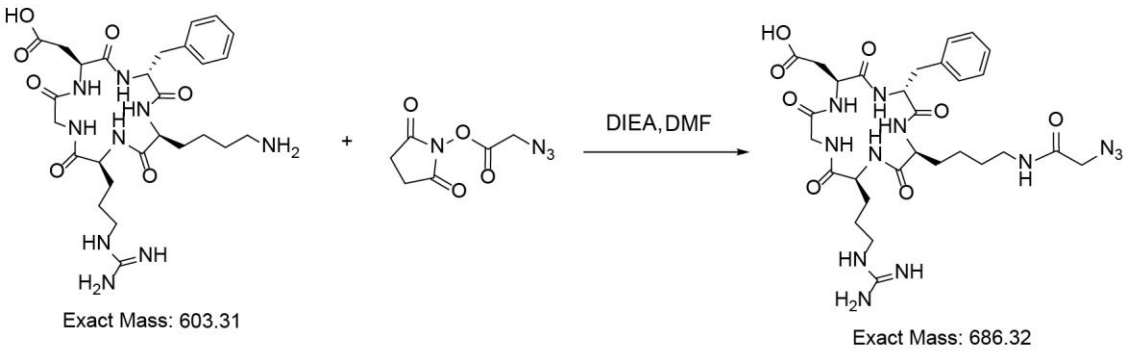

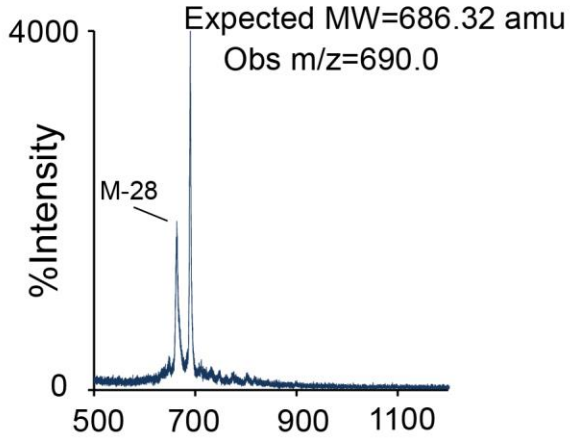

Supplementary Figure 7: **Synthesis of cRGDfK-azide ligand**

Schematic showing the chemical synthesis of cRGDfK-azide ligand and MALDI-TOF spectrum of product. The mono-azide functionalized cRGDfK product exhibits two distinct peaks in their mass spectra when analyzed using reflector mode: the parent ion ([M+]) peak and a second peak corresponding to the in-source expulsion of N_2 ([M-28]) (See Online Methods).

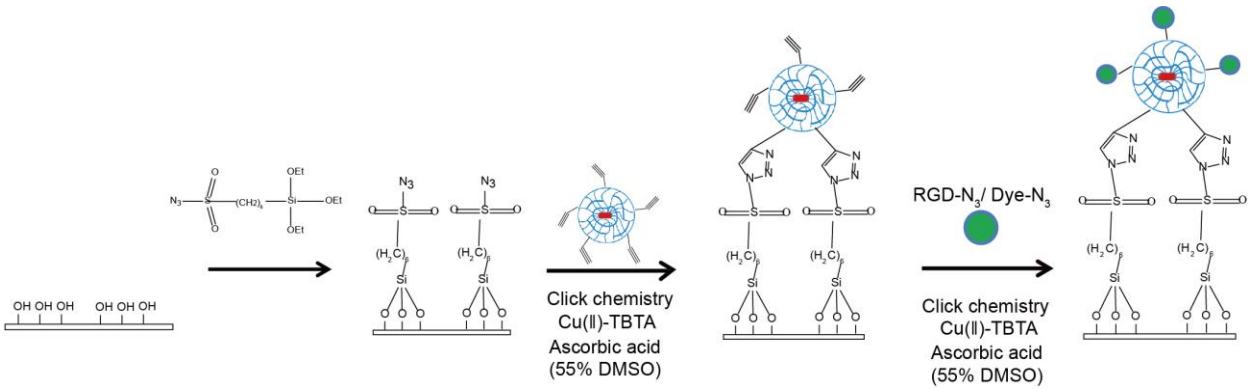

Supplementary Figure 8: OMA nanoparticles surface preparation

Schematic showing the protocol for covalent immobilization of OMA nanoparticles on glass coverslips (See Online methods).

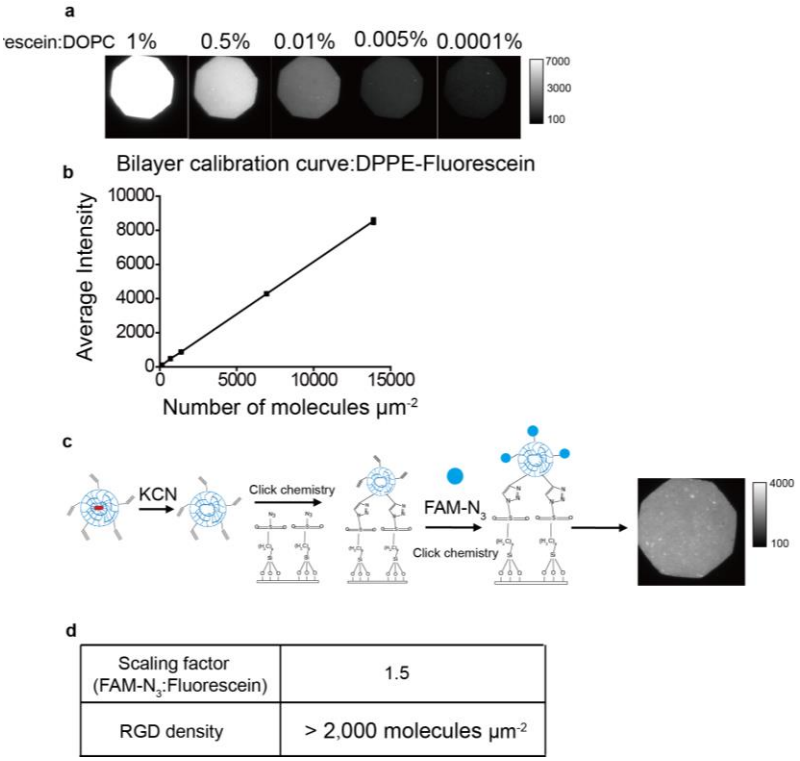

d

Scaling factor (FAM-N_3:Fluorescein)	1.5
RGD density	> 2,000 molecules µm^{-2}

Supplementary Figure 9: Determination of cRGDfK peptide density on OMA nanoparticles surface.

(**a**) Representative fluorescence images from DOPC supported lipid membranes doped with 1% to 0.0001% DPPE-fluorescein. (**b**) A plot showing the calibration curve relating the fluorescence intensity of DPPE-fluorescein doped supported lipid membranes to the molecular density. (**c**) Scheme showing the procedure used to measure the average molecules density of FAM molecules on OMAs (Au NR free) surface. (**d**) Using the calibration curve, F factor, and fluorescence intensity from FAM labeled OMA (Au NR free) functionalized coverslips; FAM density was estimated to be ~2,000 molecules µm^{-2}. Note that the absolute cRGDfK peptide density should be much higher than 2,000 molecules µm^{-2} since the cRGDfK peptide concentration is ten times greater than the FAM azide concentration during the click reaction to functionalize particles (See Online Methods).

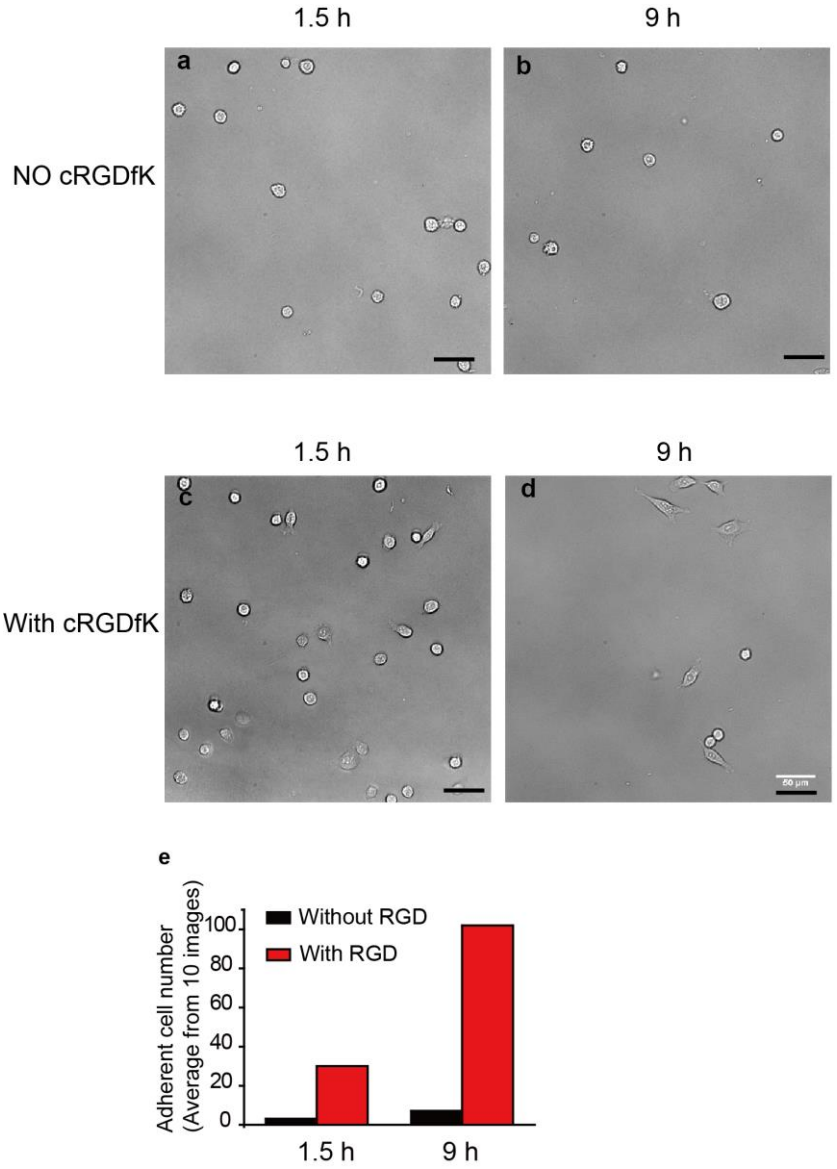

Supplementary Figure 10: Representative bright field images of NIH 3T3 cells cultured onto OMA particles surface with and without cRGDfK peptide

(**a, b**) Representative bright field images of NIH 3T3 cells cultured onto OMA nanoparticles surface lacking cRGDfK peptide. (**c, d**) Representative bright field images of NIH 3T3 cells cultured onto cRGDfK modified OMA nanoparticles surface. (**e**) The histogram displays the total number of spread of cells (from 10 images) onto OMA nanoparticles surfaces modified with (red) and without (black) cRGDfK at two time points.

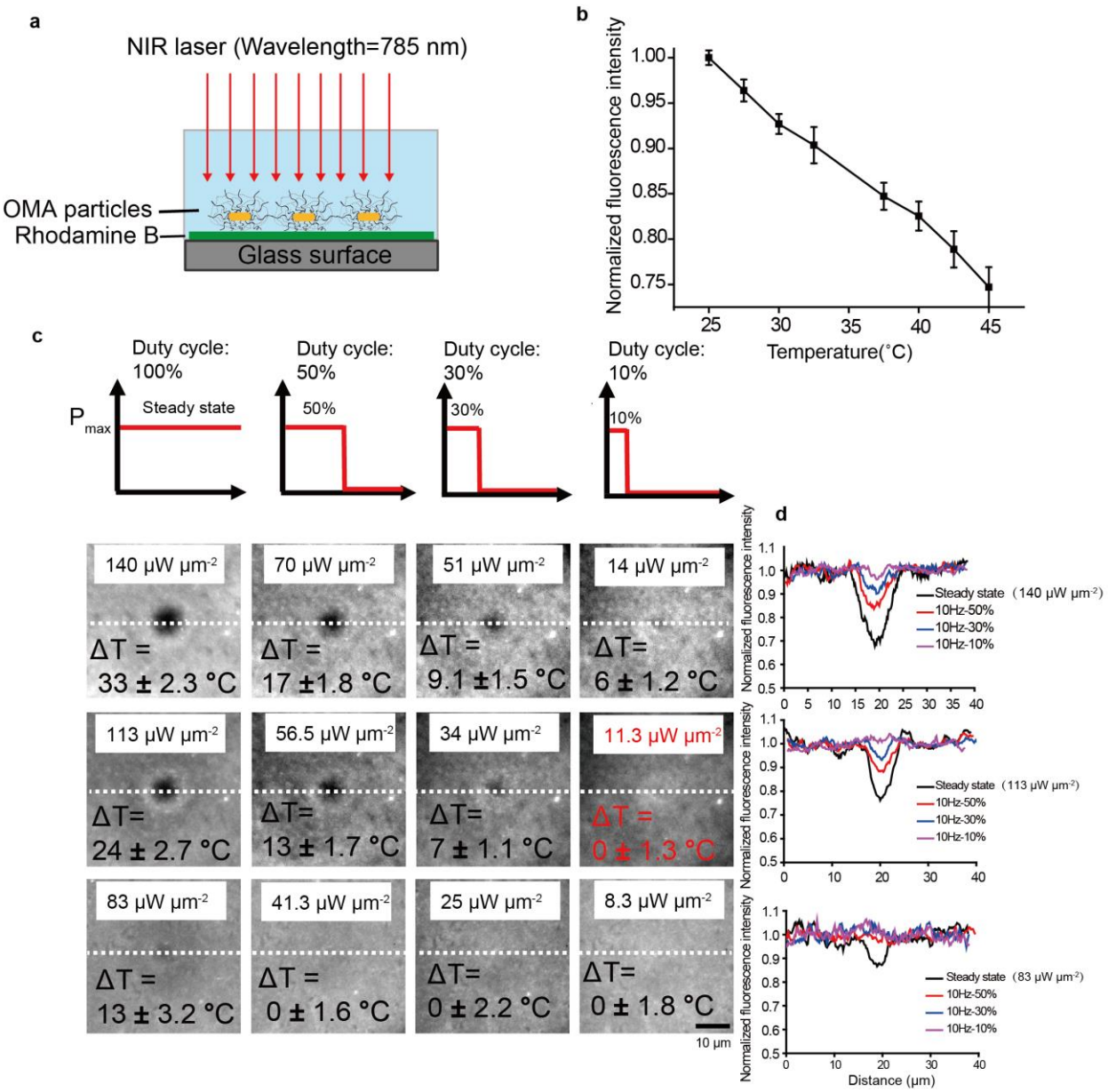

Supplementary Figure 11: Determination of OMA surface temperature

(**a**) A schematic showing the procedure used to measure the average temperature of OMA nanoparticles as a function of the NIR laser power intensity and duty cycle. First, a thin film of Rhodamine B was prepared by spin coating the glass slide with a 1 μM Rhodamine B aqueous solution. The slide was then allowed to dry slowly at ambient conditions for ~10 min. Subsequently, a few drops of a solution containing 0.1 nM OMA nanoparticles was deposited onto the Rhodamine B coated glass surface. The sample was then allowed to fully dry and then mounted into a sample holder for NIR illumination experiments in PBS. (**b**) Normalized fluorescence intensity of Rhodamine B as a function of temperature. The fluorescence curve shows that the fluorescence intensity decreases ~ 1% when temperature increases 1 °C. Data was obtained using a spectrophotometer in PBS. (**c**) Fluorescence images of Rhodamine B film coated with OMA nanoparticles and excited using different NIR laser power intensities and duty cycles. (**d**) The plot shows the normalized fluorescence intensity line scan profiles of images in (c) across the illumination area indicated by the dashed white line. Note that, at the illumination condition for cell stimulation (3.5 mW, 10% duty cycle, 10 Hz, 11.3 μW μm^{-2}, the laser spot radius is 10 μm), no detectable increase in equilibrium surface temperature was observed.

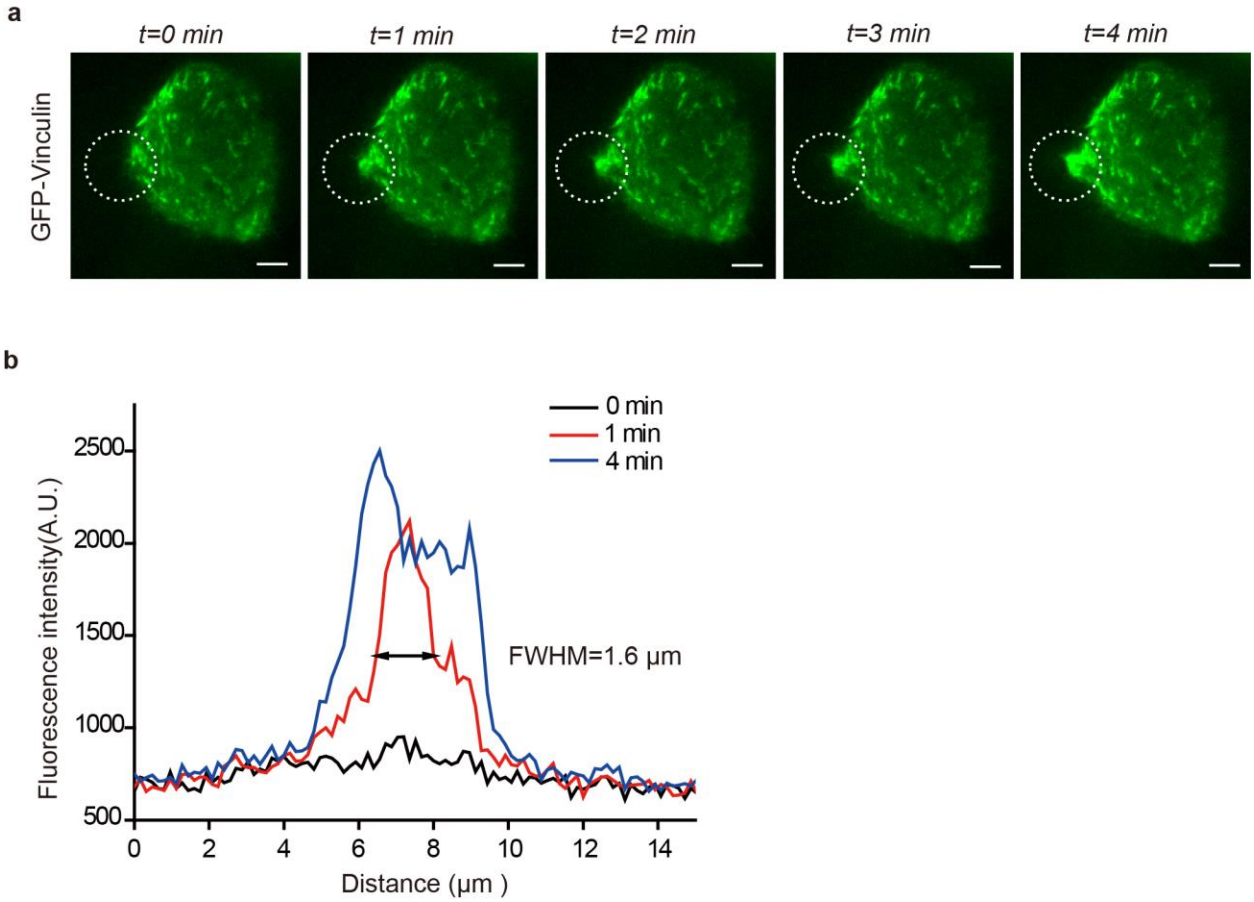

Supplementary Figure 12: Optomechanical actuation of integrin leads to GFP-vinculin recruitment
(**a**) Representative time-lapse TIRF images of GFP-Vinculin transiently transfected in 3T3 cells that were cultured on OMA nanoparticles displaying the cRGDfK peptide. NIR illumination (red dashed circle, 10 Hz, 10% duty cycle, power density = 11.3 µW µm^{-2}) leads to rapid recruitment of GFP-vinculin. Scale bars, 5 µm. (**b**) Plot represents the fluorescence intensities profiles (dashed white line) across the illumination area at different time points.

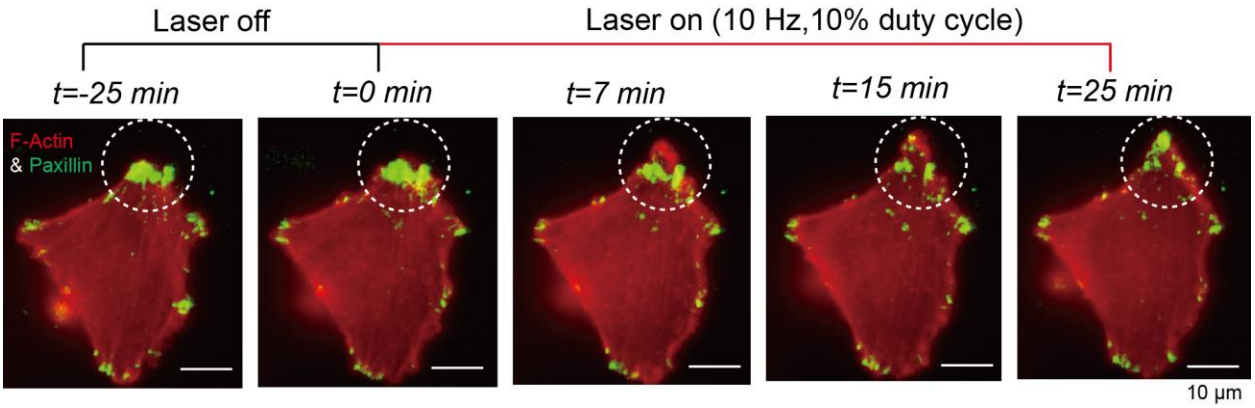

Supplementary Figure 13: Simultaneous tracking of paxillin and actin following OMA stimulation

Representative time-lapse dual-color fluorescence images of Life-Act mcherry actin (red) and GFP-paxillin (green) transiently transfected NIH 3T3 cells upon NIR illumination (white dashed circle, 11.3 μW μm^{-2}, 10 % duty cycle). Before stimulation (-25 min – 0 min), minimal changes in the actin and paxillin signal was observed. Following NIR stimulation (at t = 0 min), the cell membrane rapidly protruded toward the NIR illumination region as shown by the accumulation of Life-act mcherry within the dotted white circle (t = 7 min). At t = 15 min, puncta of GFP-paxillin were observed within the newly protruding region of the cell, thus indicating the formation of nascent focal adhesions. These nascent focal adhesions continued to grow as the NIR stimulus was maintained (t = 25 min). These dual-color fluorescence images show that the F-actin polymerization precedes the recruitment of paxillin and FA maturation upon OMA actuation.

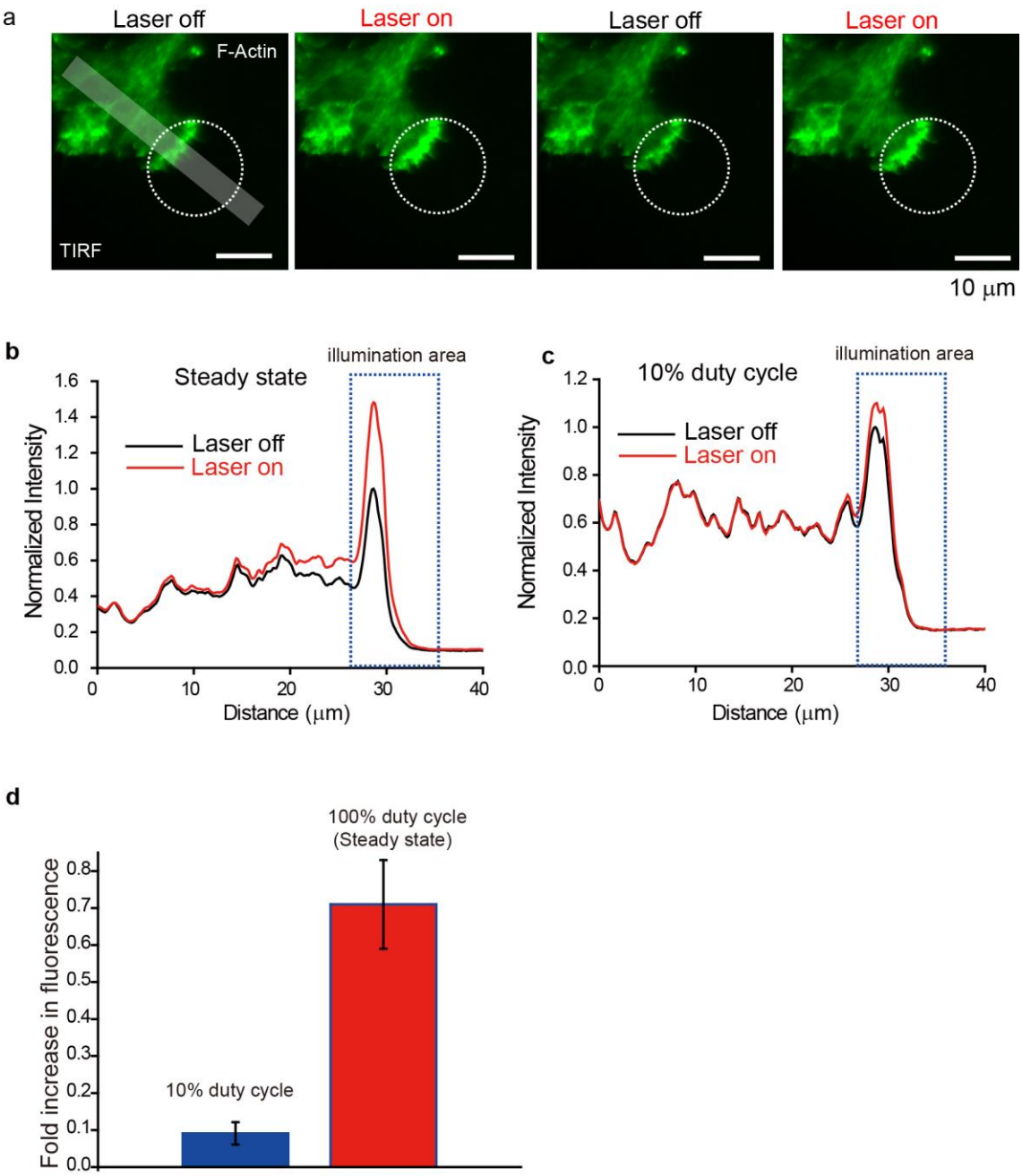

Supplementary Figure 14: Determination of F-actin displacement using TIRF-based nanometry

(**a**) Representative TIRF images of GFP-LifeAct transiently transfected 3T3 cells that were cultured on OMA nanoparticles when the NIR laser (red dashed circle, 111 μW μm^{-2}, 100% duty cycle) was switched on and off. The acquisition time was 1 s. (**b**-**c**) Plots show fluorescence line scan analysis from the region denoted by the gray rectangle in the TIRF image shown in (**a**). The red and black profiles represent the TIRF intensity when NIR was switched on and off. The NIR laser was operated at 100% duty cycle in (**b**), and at 10% duty cycle in (**c**). The illumination area was indicated by dashed blue rectangle. (**d**) Plot displays the average fold increase in TIRF signal in the illumination area when OMA nanoparticles were excited by NIR laser with 10% duty cycle and 100% duty cycle, respectively. The error bar for each data point represents the standard deviation of cell response from *n*= 6 cells.

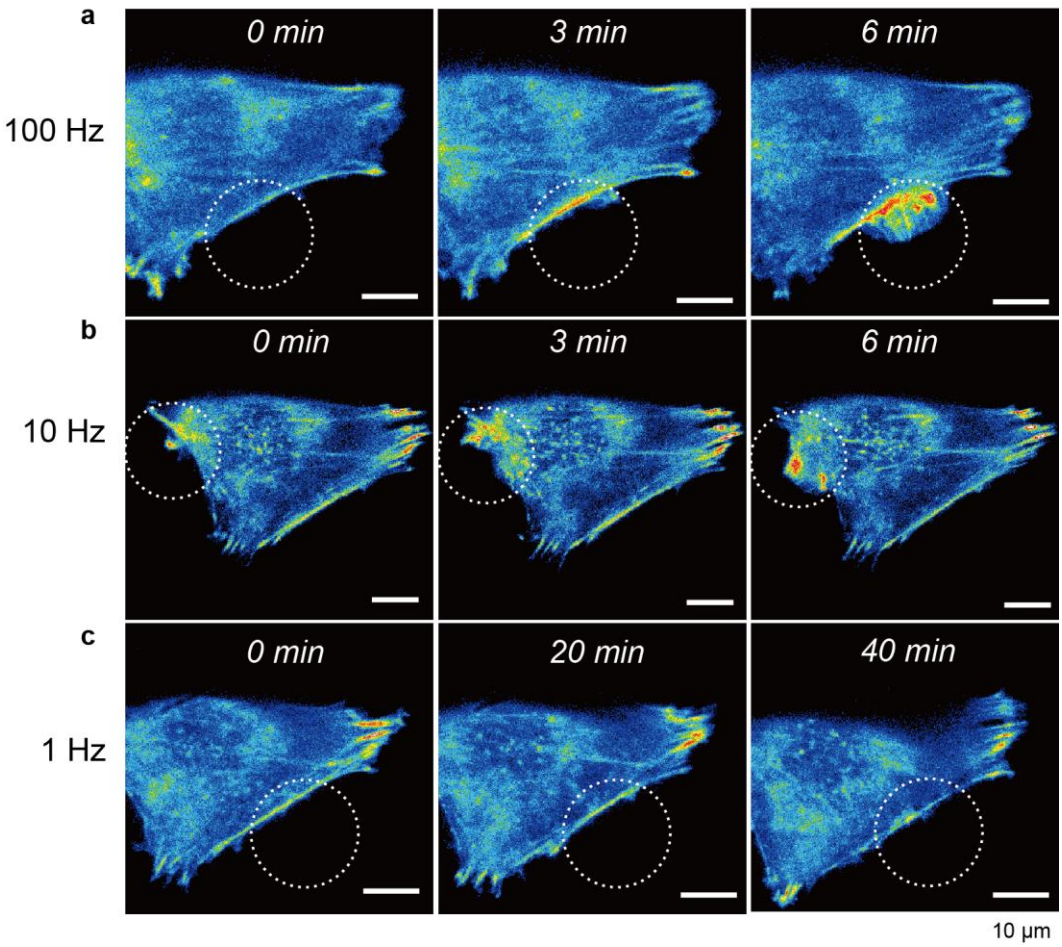

Supplementary Figure 15: Cell response to NIR illumination frequencies from 1 Hz to 100 Hz

Representative time-lapse fluorescence images of Life-act-mCherry transiently transfected NIH 3T3 cells upon NIR illumination at different frequencies from 1 Hz to 100 Hz. Cells were cultured overnight prior to stimulation.

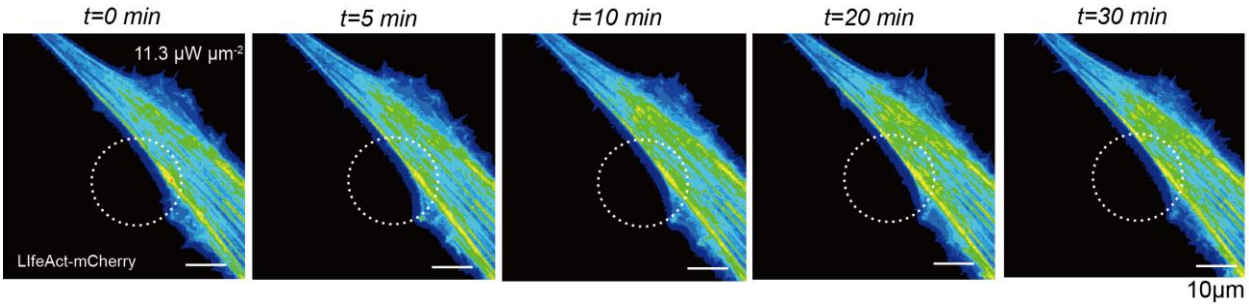

Supplementary Figure 16: Cell response to continuous NIR illumination
Representative time-lapse fluorescence images of LifeAct-mCherry transiently transfected NIH 3T3 cells upon continuous NIR illumination (power density = 11.3 μW μm^{-2}, the duty cycle is 100%). No significant change in F-actin was observed under these experimental conditions. This suggests an important role in cyclic application of mechanical stimulus for driving integrin activation.

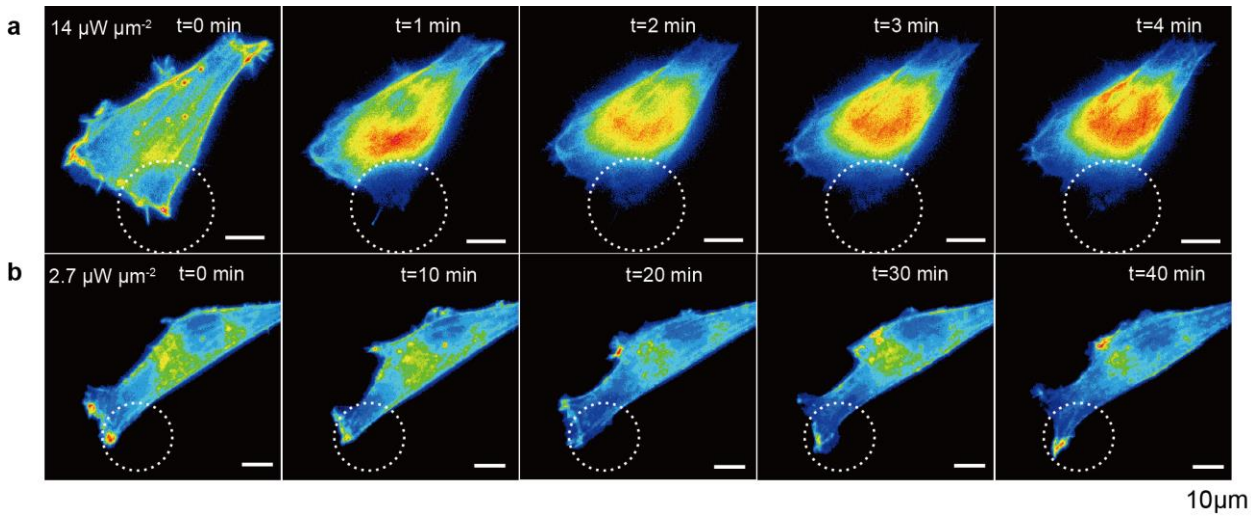

Supplementary Figure 17: Cell response to high and low intensity NIR illumination
Representative time-lapse fluorescence images of Life-act mcherry transiently transfected NIH 3T3 cells cultured on OMAs surface upon high (14 µW µm^{-2}) (**a**), and low intensity (2.7 µW µm^{-2}) (**b**) NIR illumination. Scale bars: 10 µm.

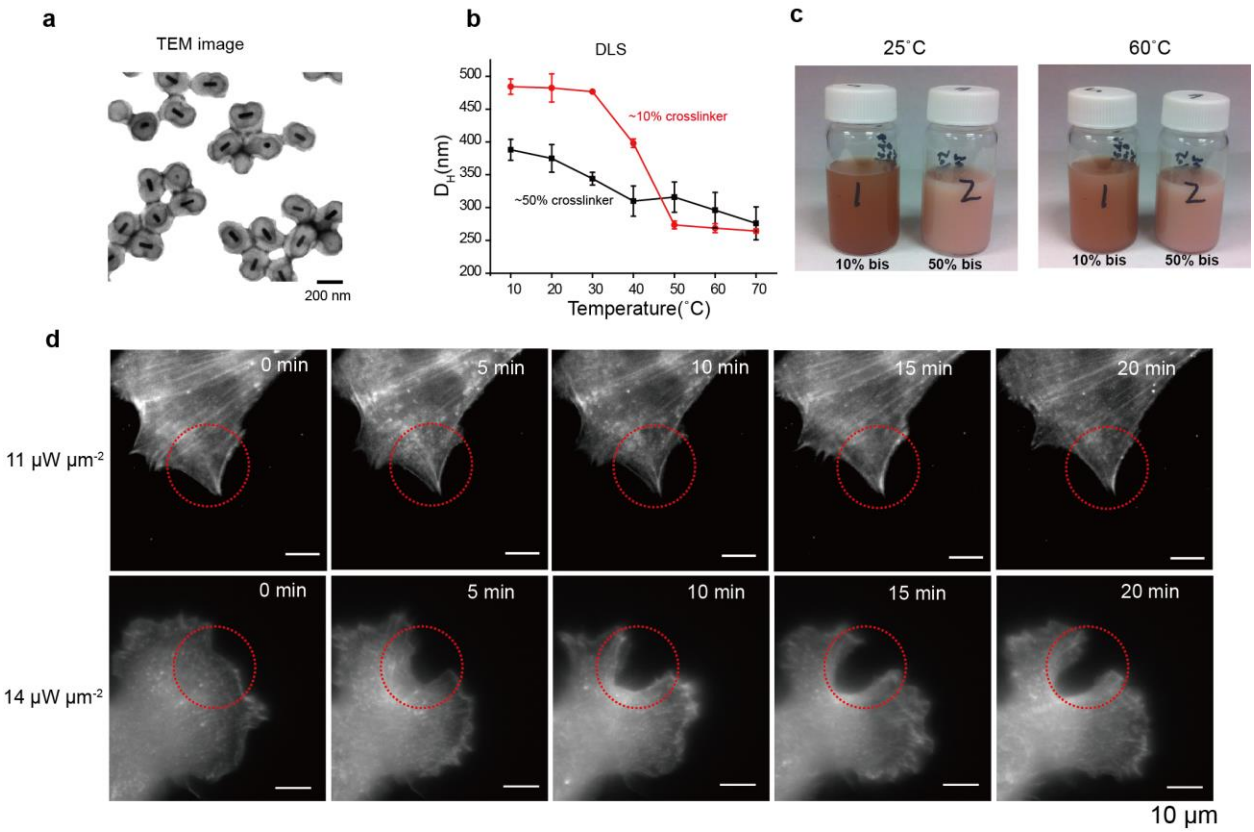

Supplementary Figure 18: Control OMA particles synthesized with 50% crosslinking *N,N′*-Methylenebis(acrylamide) to test potential thermal effects.
(**a**) Representative TEM image of Au nanorod core-NIPMAm shell nanoparticles generated using a 50% cross-linker concentration (N,N-Methylenebisacrylamide). (**b**) Temperature-controlled DLS measurements reporting the hydrodynamic diameter of core-shell nanoparticles with 10% cross-linker (red) and 50% cross-linker concentration (black) as a function of temperature. (**c**) Photographs of aqueous solutions containing core-shell nanoparticles with 10% and 50% crosslinker concentration at different temperatures. (**d**) Representative time-lapse fluorescence images of Lifeact-mCherry transiently transfected NIH 3T3 cells cultured on the 50% cross-linker concentration particles upon NIR illumination with different laser power densities. Cells were cultured overnight prior to stimulation. The duty cycle was 10% and actuation frequency was 10 Hz in these experiments.

The cross-linker concentration in thermo-responsive polymers can strongly alter their properties[23]. The increased crosslinking density significantly reduced the swelling ratio of polymer particles as shown in the temperature controlled DLS measurement (b). The average hydrodynamic diameter of the core-shell nanoparticles with 50% crosslinker was reduced from 370 ± 20 nm to 260 ± 30 nm. This volume transition is significantly reduced compared with particles crosslinked with 10% *N,N′*-methylenebisacrylamide. The dampened volume transition is also shown in (c). Importantly, core-shell particles with 50% crosslinker failed to display an increase in actin localization regardless of the NIR intensity tested.

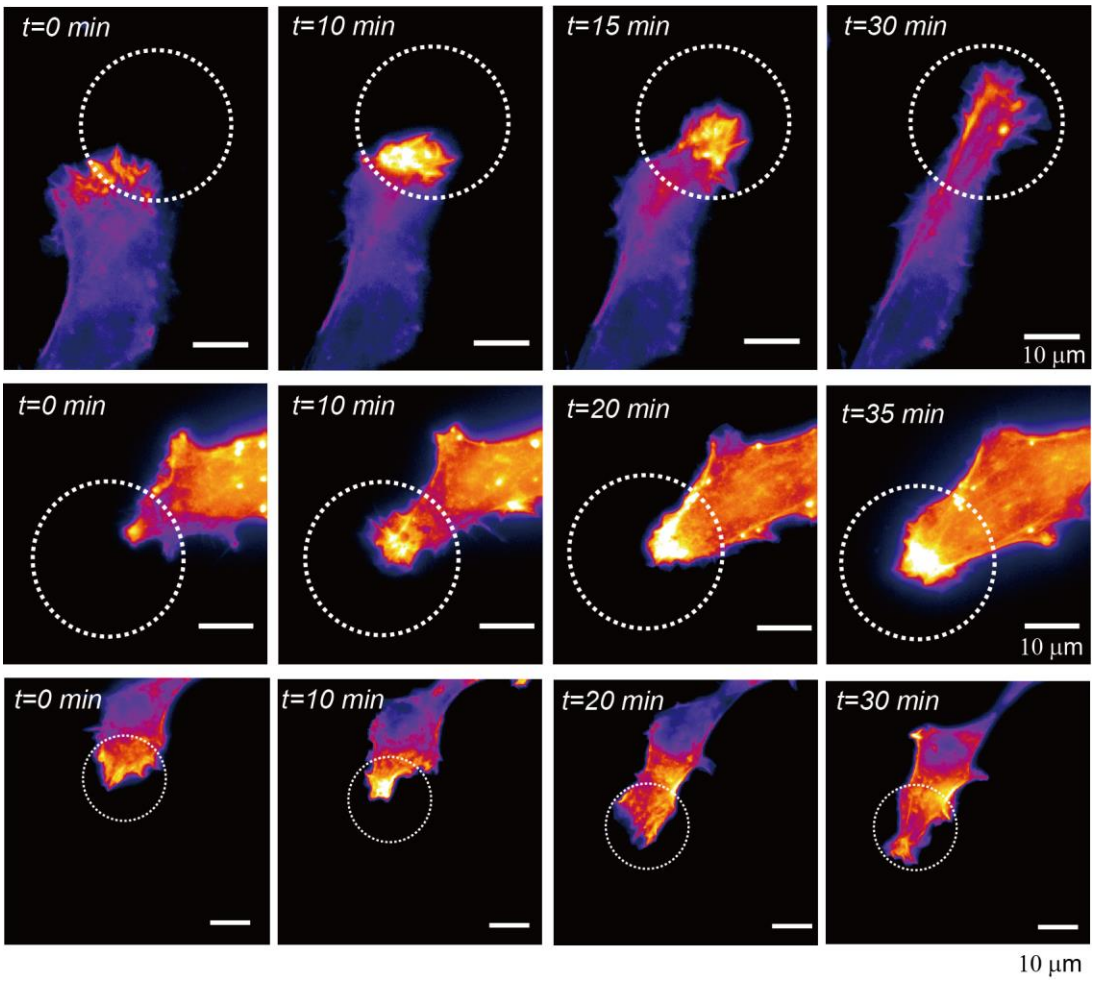

Supplementary Figure 19: OMA control of NIH 3T3 cell migration.
Representative fluorescence images taken from time-lapse videos of OMA control of NIH 3T3 cell migration. Cells were transfected with Life-Act mCherry. The white dashed circle represents the region of NIR illumination.

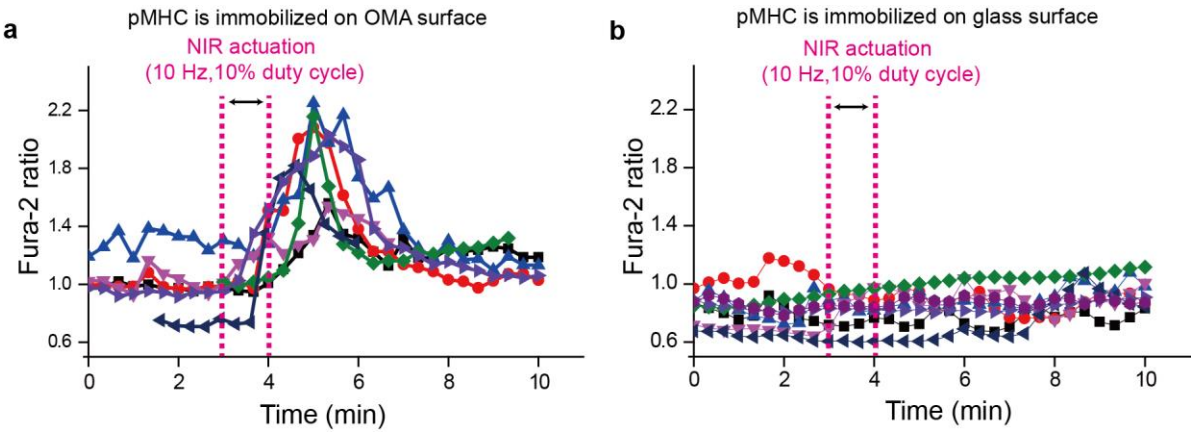

Supplementary Figure 20: Quantitative analysis of fura-2 ratio rise for T cells on different surfaces upon NIR stimulation.

(a-b) Plots depicting a histogram showing the quantitative analysis of fura-2 ratio rise for different T cells upon OMA stimulation as depicted in (**Fig. 3e**) and (**Fig. 3g**). *n*= 7 cells for each plot.

Supplementary Note

Upon OMA particle collapse, the polymer will increase in stiffness and the density of the RGD ligands will also likely increase. Note however that the collapsed state of the OMA particles is transient persisting for 10 ms within each 100 ms time window (one period). This indicates that the NIR illumination in our experiments causes a transient change to the rigidity of the particle and the density of RGD. Given that the Young's modulus of PNIPMAm is reported to increase from 100 kPa to 600 kPa upon collapse[32], this equates to a change in the rigidity of the surface from 100 to 150 kPa (10% × 600 + 90% ×100). Based on literature precedent, an increase in rigidity from 100 to 150 kPa is insignificant, and will not impact cell response[33-35]. In addition, NIR illumination is tuned such that each particle is partially collapsed and surface temperature of the OMA particles does not exceed the LCST. Therefore, the stiffness is likely less than 150 kPa during NIR actuation.

In regards to the change in RGD density, we measured the RGD density and determined that it is more than 2,000 peptides μm^{-2} (**Supplementary Figure 9**) which is 5 fold greater than the threshold required to trigger FA formation[36]. Based on literature precedent there is minimal difference in cell response to densities that exceed this threshold value[36]. Therefore, it is highly unlikely that a transient increase in RGD density would drive the cell response.

Finally, ROCK inhibitor studies (**Fig. 2b**) show that the cell response is maintained, further confirming that the mechanism is independent of cell stiffness sensing mechanisms.
Taken together, these lines of evidence indicate that the change in RGD density and change in particle stiffness do not contribute to the observed cell response.

Table: OMA particle size change determination.

Technique	***Observation***	***Experimental condition***
sCMOS high-speed fluorescence measurements recording particle dynamics **(Fig. 1f)**	<100 nm decrease in particle diameter (FWHM)	NIR illumination: 11 μW μm^{-2}, 10 Hz frequency,10% duty cycle. Conditions: water, 37 ℃.
Liquid cell temperature-controlled AFM measurements **(Fig. 1c and d)**	~120 nm decrease in particle diameter (FWHM)	Steady state temperature control Conditions: water, variable temperature
SIM microscopy **(Supplementary Figure 3)**	~100 nm decrease in particle diameter (FWHM)	Continuous NIR illumination, 11 μW μm^{-2} Conditions: water, 37 ℃
TIRF-based nanometry **(Supplementary Figure 14)**	100 nm ± 10 nm decrease in particle height	NIR illumination condition: 11 μW μm^{-2}, 10 Hz frequency, 10% duty cycle. Conditions: HEPES buffer, 37 °C

32. Schmidt, S. et al. *Adv. Funct. Mater.* **20**, 3235-3243 (2010).
33. Yeung, T. et al. *Cell Motil. Cytoskeleton* **60**, 24-34 (2005).
34. Elosegui-Artola, A. et al. *Nat. Mater.* **13**, 631-637 (2014).
35. Plotnikov, S.V., Pasapera, A.M., Sabass, B. & Waterman, C.M. *Cell* **151**, 1513-1527 (2012).
36. Arnold, M. et al. *Chemphyschem* **5**, 383-388 (2004).